Colloids and Surfaces A: Physicochemical and Engineering Aspects 678 (2023) 132481

Contents lists available at ScienceDirect

Colloids and Surfaces A: Physicochemical and Engineering Aspects

journal homepage: www.elsevier.com/locate/colsurfa

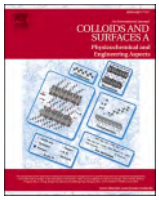

Tailoring the adsorption behaviors of flucytosine on B_nN_n (n = 12, 16, 20, and 24) nanocage scaffolds: A computational insight on drug delivery applications

Xiaocong Yao [a,1], Ji Mu [b,1], Yi Zheng [b], Jiang Wu [b], Weihua Zhu [c], Kun Wang [b,*]

[a] Department of Osteoporosis Care and Control, The Xiaoshan Affiliated Hospital of Wenzhou Medical University, Hangzhou, Zhejiang 311200, China
[b] School of Pharmaceutical Sciences, Wenzhou Medical University, Wenzhou 325035, China
[c] Institute for Computation in Molecular and Materials Science, School of Chemistry and Chemical Engineering, Nanjing University of Science and Technology, Nanjing 210094, China

HIGHLIGHTS

- The adsorption behaviors of flucytosine (Fcy) onto B_nN_n (n = 12, 16, 20, and 24) were studied.
- The partially covalent B···N bond is investigated to be the main force between Fcy and B_nN_n.
- Large reductions in the HOMO-LUMO energy gap were observed for all B_nN_n-Fcy complexes after Fcy adsorption.
- The interaction energy between the entities and the adsorption capacity of B_nN_n diminishes with the increase in cage size.

GRAPHICAL ABSTRACT

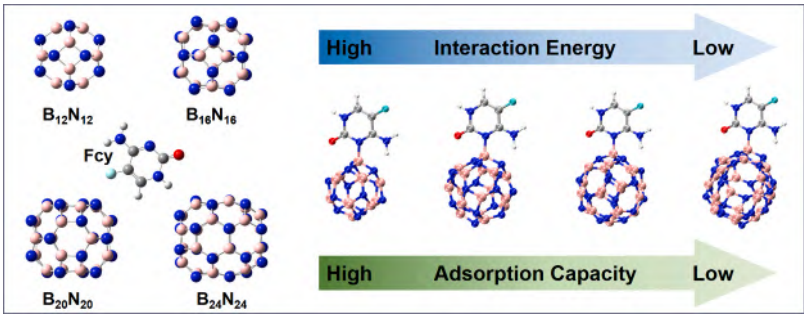

ARTICLE INFO

Keywords:
Flucytosine
Boron nitride
Surface adsorption
DFT
Molecular dynamics

ABSTRACT

Understanding the interactions between boron nitride-based nanocage scaffolds with drug molecules is a prerequisite for their application as drug carriers. Herein, the adsorption behaviors of the anti-fungal drug flucytosine (Fcy) on the surfaces of different zero-dimensional B_nN_n (n = 12, 16, 20, and 24) nanomaterials were systematically studied based on the density functional theory (DFT) and molecular dynamics (MD). An ideal complementarity between their electrostatic potential surface is witnessed for the most stable B_nN_n-Fcy complexes. The atoms in molecules (AIM) analysis further reveals the partially covalent B···N bond is the main force between Fcy and B_nN_n. And the interaction energy between the entities in both gas and aqueous phase diminishes with the increase of cage size. Meanwhile, significant reductions in the HOMO-LUMO band gap energy of B_nN_n-Fcy complexes were observed after Fcy adsorption. Furthermore, MD simulations demonstrate the spontaneous adsorption of Fcy molecules onto the surface of B_nN_n, with the adsorption capacity of B_nN_n decreasing as the cage sizes increase. The aforementioned findings collectively indicate the adsorption behavior of Fcy can be tailored by the selection of different B_nN_n, making it a potential candidate for Fcy drug delivery to meet different needs.

* Corresponding author.
E-mail address: wangkun@wmu.edu.cn (K. Wang).
[1] These authors contributed equally to this work.

https://doi.org/10.1016/j.colsurfa.2023.132481
Received 8 September 2023; Received in revised form 27 September 2023; Accepted 28 September 2023
Available online 29 September 2023

Hopefully, the results would provide valuable theoretical guidance for the development of B_nN_n-based drug delivery systems.

1. Introduction

Diseases caused by various fungal infections have become a serious threat to human health all over the world. Fungi cause various diseases in humans, from allergic syndromes to superficial, disfiguring, and life-threatening invasive fungal diseases, which collectively affect over 1 billion people worldwide [1–3]. Pharmacotherapy is definitely an important and dominate treatment for fungal infections, among which flucytosine (Fcy) is the preferred high-dose drug owing to its high sensitivity to systemic fungal infections caused by *candida* and *cryptococcus* [4,5]. However, the rapid dissolution and almost complete absorption of Fcy may result in severe side effects, especially liver toxicity, ranging from mild liver damage to fulminant liver failure [6,7]. Even worse, the narrow treatment window and the fact that 90% of the drug is excreted from the urine through glomerular filtration require frequent administration [8], leading to poor patient compliance and ultimately affecting its effectiveness in clinical use. In fact, this is also a common issue faced by many drugs, such as isoniazid, pyrazinamide, and so on [9]. Therefore, in order to address the problems encountered by Fcy, the administration strategy of existing drugs needs to be improved to strengthen their efficacy while reducing their toxicity.

The boosting of nanotechnology renders nanomaterials a promising and popular candidate for controllable drug delivery systems. Nanomaterials can not only improve the solubility of poorly water-soluble drugs and prolong the half-life of drugs, but also release the drug in a controlled or environmentally responsive manner to regulate the biological distribution of drugs and thus minimize side effects [10,11]. In recent decades, various nanomaterials have been developed and adopted as drug delivery vehicles, especially these low-dimensional nanomaterials based on carbon and boron nitride (BN), such as fullerenes, graphene derivatives, boron nitride nanocages and so on [11,12]. Among them, BN nanocages with different sizes have been repeatedly studied for varied applications (*e.g.*, drug delivery and biosensors) due to their superior biocompatibility, remarkable stability as well as excellent physical and chemical properties [13–23]. For example, the potential applications of $B_{12}N_{12}$ for serine [18], penicillamine [19], cladribine [20] and ciclopirox [17] were computationally investigated. Recently, our group has theoretically demonstrated that $B_{12}N_{12}$ can serve as an ideal carrier for the anti-tuberculosis drug pyrazinamide[16]. Gao et al. indicated that the glycine- functionalized boron nitride ($B_{12}N_{12}$/$B_{16}N_{16}$) nanocages are promising materials for biomedical and drug-delivery applications based on density functional theory (DFT) calculations [24]. Hazrati et al. proposed the potential application of $B_{24}N_{24}$ as a drug delivery system for the anticancer drug 5-fluorouracil [25].

It is generally believed that the size of nanomaterials has significant effects on the adsorption behaviors of drug molecules. Moreover, a thorough knowledge of the interaction between nanomaterials and drug molecules is a prerequisite for their applications. Nevertheless, the adsorption behaviors of Fcy onto the BN nanocages remains unknown, nor the influence of different sizes of nanostructures on their interaction with Fcy. Hence, it is of great importance to monitor the adsorption behaviors of Fcy on the surfaces of zero-dimensional B_nN_n materials with various sizes. Herein, based on the density functional theory (DFT), our results demonstrated that different sizes of B_nN_n have significantly different structural and electronic properties. And the geometric parameters, bonding nature, and interaction energy of the most stable B_nN_n-Fcy (n = 12, 16, 20, and 24) complexes display a pronounced dependence on the size of B_nN_n. Additionally, the results from molecular dynamics (MD) simulations indicate that Fcy molecules were spontaneously adsorbed on the surface of B_nN_n. And the adsorption capacity of B_nN_n for Fcy decreases as cage sizes increase, which is also applicable for antiviral favipiravir (FPV) and anti-tuberculous isoniazid (INH) drugs. Expectantly, our results would enrich the knowledge of the adsorption behavior of flucytosine on different zero-dimensional B_nN_n materials and provide meaningful guidance for the development of nanocage-based drug delivery systems.

2. Computational details

2.1. DFT calculations

The geometric structures of flucytosine and pristine B_nN_n (n = 12, 16, 20, and 24) were fully optimized in Gaussian 09 program [26] at the M06–2X/6–311G** level, the method of which is extensively adopted and has been shown reliable in dealing the similar systems [16–18]. The most stable configuration of Fcy on the surface of different B_nN_n (n = 12, 16, 20, and 24) was obtained by a conformation search method as described previously [16,27]. Concretely, 500 structures with Fcy randomly distributed around the B_nN_n were optimized at the PM6-D3H4 level using MOPAC2016 software [28], which were generated by the Molclus package [29]. Then, according to the energy sequence of the complexes and the potential interaction sites derived from the electrostatic potential surface of each component, several conformers were selected for DFT calculations at the M06–2X-D3/6–311G** level. Besides, only neutral systems (q = 0) with the singlet state were considered in this study, as the singlet structure is demonstrated to be the lowest-energy isomer for the similar system by the previous study [15]. Meanwhile, the frequency calculations were conducted to ensure all the optimized structures are at local minima on the potential energy surface and represent no imaginary frequencies. Finally, the structure with the lowest Gibbs free energy is regarded as the most stable configuration at the current calculation level.

To investigate the structural stability of each B_nN_n nanocage, the cohesive energy of the pristine B_nN_n can be determined by the following equation:

$$E_{coh} = [E_{BnNn} - nE_B - nE_N)]/(2\ n) \quad (1)$$

where E_B, E_N, and E_{BnNn} are the electronic energy of a single B atom, N atom and B_nN_n molecule, respectively; n is the number of the corresponding atoms involved in system. And the interaction energy (E_{int}) between Fcy and B_nN_n in gas phase can be computed though the equation bellow:

$$E_{int} = E_{complex} - (E_{BN} + E_{Fcy}) + E_{BSSE} \quad (2)$$

where $E_{complex}$ represents the total energy of the B_nN_n-Fcy complex, E_{BN} and E_{Fcy} are the energy of B_nN_n and Fcy, respectively; E_{BSSE} is the basis set superposition error (BSSE) energy, which was computed by the Boys-Bernardi counterpoise procedure [30]. Moreover, the polarizable continuum model (PCM) was adopted to imitate the solvent effect of water on the adsorption of Fcy drug [31], with the interaction energy ($E_{int\text{-}w}$) in aqueous phase calculated based on Eq. (2) without applying BSSE correction.

The frontier molecular orbitals, including the highest occupied molecular orbital (HOMO) and the lowest unoccupied molecular orbital (LUMO), are important indicators for describing the chemical reactivity and ability of molecules to adsorb on a specific surface. On the basis of the calculated HOMO energy (E_{HOMO}) and LUMO energy (E_{LUMO}), the HOMO-LUMO energy gap ($E_{bg} = E_{LUMO} - E_{HOMO}$) can be obtained, which is always positive for the studied systems here. Considering the calculated HOMO-LUMO energy gap is greatly affected by the selected DFT functionals, the B3LYP functional was employed to calculate E_{bg} of B_nN_n

and their complexes as it is proved to be an ideal functional to cope with the similar systems [32,33]. Meanwhile, the relevant quantum molecular descriptors are calculated to predict the physical and chemical properties of the system using the formula below:

$$\mu = \frac{E_{HOMO} + E_{LUMO}}{2} \tag{3}$$

$$\eta = \frac{E_{LUMO} - E_{HOMO}}{2} \tag{4}$$

$$S = \frac{1}{2\eta} \tag{5}$$

$$\omega = \frac{\mu^2}{2\eta} \tag{6}$$

where μ represents chemical potential, η is chemical hardness, S is global softness and ω stands for electrophilicity index.

The quantum theory of atoms in molecules (AIM) method was employed to analyze the electron density and bonding characteristics of the Fcy-B_nN_n complexes. The topological parameters at the bond critical points (BCPs), such as electron density (ρ), Laplacian of electron density ($\nabla^2\rho$), Lagrangian kinetic energy (G_r), potential energy density (V_r) and total energy density (H_r) are expected to understand and identify the type of interactions [34]. In addition, the AIM analyses were done in Multiwfn 3.8 software [35], and the results were visualized using VMD [36].

2.2. Molecular dynamics simulations

For deciphering the adsorption details and measuring the adsorption capacity of Fcy on different B_nN_n nanocages, MD simulations of B_nN_n (n = 12, 16, 20, and 24) nanocages interacting with Fcy in aqueous solutions were carried out using the GROMACS 2021 computational package [37]. The initial configurations of B_nN_n (n = 12, 16, 20, and 24) and Fcy were taken from the DFT optimized structure, and the force field parameters were generated using Sobtop package [38]. The cubic simulation boxes were constructed by the Packmol program [39] with the periodic boundary conditions applied to the x, y, and z directions, which contain one B_nN_n molecule located in the center and 50 randomly distributed Fcy molecules, solvated by 5000 water molecules. The general AMBER force field (GAFF) [40] was employed to describe all of the bonded and non-bonded interactions, and the atom charges were calculated based on the framework of the advanced restrained electrostatic potential (RESP) charges method [41] by Multiwfn software [35]. For H_2O molecules, the TIP3P water model was adopted. The electrostatic interactions were computed using PME methods with a cut-off distance of 1 nm [42]. Energy minimizations were conducted using the conjugate gradient descent method to dismiss the initial stress and obtain a reliable initial configuration. Following a 1 ns equilibration simulation, the production simulations ran for 20 ns with a time step of 2 fs in the NPT ensemble. In the production runs, the temperature was kept constant at 298.15 K by the velocity-rescale thermostat [43] and the pressure was maintained at 1 atm by Parrinello-Rahman barostat [44]. From the simulated data, structural and dynamic properties were analyzed directly by the GROMACS post-processing tools, and all the visualization was processed using the VMD program [36].

3. Results and discussion

3.1. Structure and properties of Fcy and pristine B_nN_n nanocages

The optimized structures of different B_nN_n (n = 12, 16, 20, and 24) nanocages and Fcy are shown in Fig. 1. Structurally, all B_nN_n nanocages possess high symmetry of T_h, T_d, $C_{4\,h}$, and S_8, respectively. $B_{12}N_{12}$

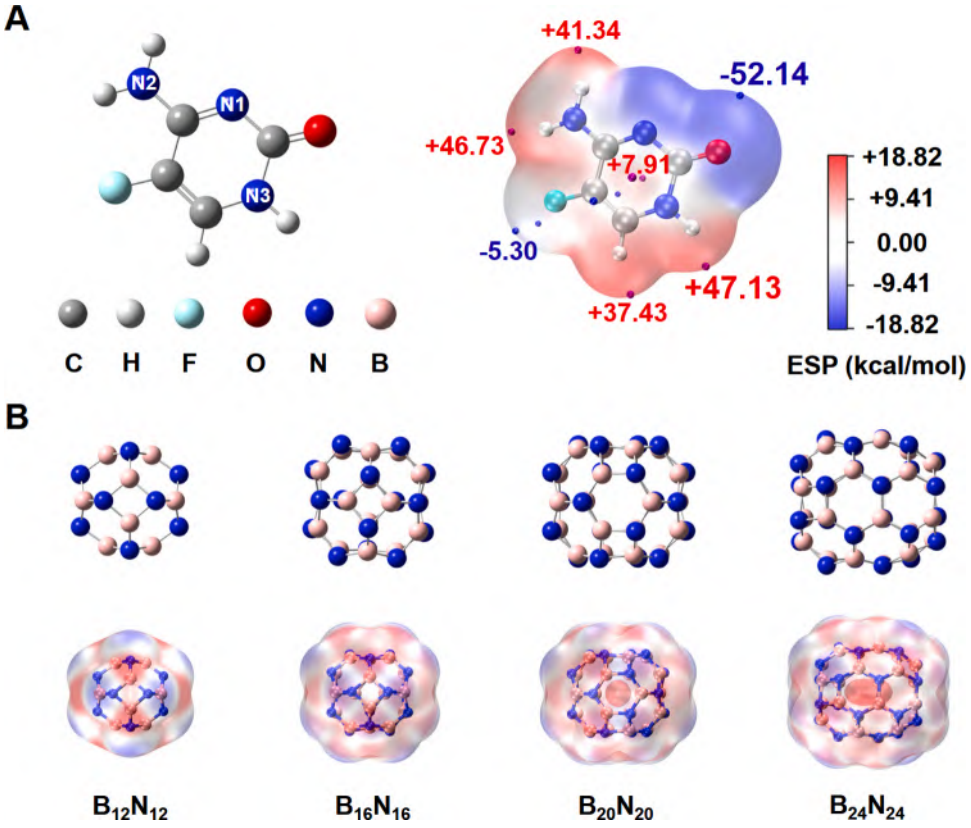

Fig. 1. The optimized structures and the ESP mapped vdW surface of (a) Fcy drug and (b) different B_nN_n (n = 12, 16, 20 and 24). The surfaces are defined as an electron density (ρ) equal to 0.001 au. The purple and blue dot stands for the local maxima and minima of ESP on the vdW surface of Fcy, respectively.

includes eight hexagons and six squares, while $B_{16}N_{16}$ is composed of twelve hexagons and six squares. Both $B_{20}N_{20}$ and $B_{24}N_{24}$ have more than one isomer, only the most stable configuration was considered here. The most stable $B_{20}N_{20}$ has two octagons, twelve hexagons and eight squares, while the most stable $B_{24}N_{24}$ is composed of two octagons, sixteen hexagons and eight squares. Additionally, the calculated structures here are in good agreement with previous literatures [45–47]. Also, the cohesive energies of B_nN_n (n = 12, 16, 20, and 24) were calculated to elucidate the geometric stability of these nanocages, which was as large as − 6.07, − 6.22, − 6.27, and − 6.34 eV/atom, respectively. The negative and high value of cohesive energy suggested the high structural stability of pristine B_nN_n, which are consistent with previous studies, such as − 6.09 eV/atom for $B_{12}N_{12}$ [48].

The electrostatic potential (ESP) mapped vdW surface is widely adopted for predicting the interaction sites and investigating electrostatic interactions between molecules as it can depict the charge distributions on the molecular surface. Generally, atoms with higher positive ESPs have a larger probability to become donor sites whereas atoms with lower negative ESPs are expected to be better acceptor sites. As illustrated in Fig. 1**A**, the negative ESPs for Fcy almost distribute near the O and N1 atoms; and the positive ESPs mainly locate around the H atoms. Specifically, the global minima and maxima of ESPs on the vdW surface are − 52.14 and + 47.13 kcal/mol, which correspond to the O and H (linked to the heterocyclic N atom) atoms, respectively. Meanwhile, the surface area in different ESP ranges of four B_nN_n is plotted as shown in Fig. 2**A**, which demonstrates that the absolute value of the positive ESP is larger than that of the negative ones for all B_nN_n. And the negative EPSs of all B_nN_n nanocages (blue regions) are mainly distributed on the N atoms, while the positive ones (red regions) are concentrated on the B atoms. The above data suggests Fcy prefers to interact with the B atoms of B_nN_n nanocages through its N and O atoms. Besides, by comparing the statistical data in Fig. 2**A**, it can be found that the surface area of most ESP ranges for different B_nN_n follows the order of $B_{24}N_{24} > B_{20}N_{20} > B_{16}N_{16} > B_{12}N_{12}$, while for the ESP range around 29 kcal/mol, the order is reversed. Considering that the higher ESP regions (around 45 kcal/mol and 53 kcal/mol) for $B_{20}N_{20}$ and $B_{24}N_{24}$ are located in the middle of the molecules (the darker red region as shown in Fig. 1**B**), which will not be accessed by other molecules, the ESP region of 29 kcal/mol in B_nN_n would be the most ideal interaction site. And the higher surface area of 29 kcal/mol ESP region may indicate stronger interactions. Hence, the interaction energy between Fcy and B_nN_n may decrease as the nanocage size increases.

The size of different boron nitride nanocages can be characterized by their volume and total surface area. Based on the vdW surface defined by electron density (ρ) equal to 0.001, 0.002 and 0.003 au isosurface, the vdW surface area (*Sa*) and the molecular vdW volume (*V*) can be quantified respectively and the results are shown in Table 1. No doubt that both volume and surface area follow the order: $B_{24}N_{24} > B_{20}N_{20} > B_{16}N_{16} > B_{12}N_{12}$. For example, at ρ = 0.001 au isosurface, the *Sa* for different B_nN_n (n = 12, 16, 20, 24) are 208.65, 249.12, 300.25 and 343.75 Å^2 and the *V* are 264.03, 345.04, 432.60 and 513.64 Å^3, respectively. Additionally, specific surface area (SSA), defined as *Sa/V*, can also be computed from these data and pictured in Fig. 2**B**. At ρ = 0.001 au isosurface, the calculated SSA for B_nN_n (n = 12, 16, 20, 24) are 0.790, 0.722, 0.694 and 0.669 Å^2/Å^3, respectively. Obviously, smaller B_nN_n nanocages have a relatively larger specific surface area.

According to the frontier orbital theory, the E_{HOMO} reflects the ability of a molecule to donate electrons and thus can be regarded as a measure of nucleophilicity; whereas the E_{LUMO} depicts the molecular ability to accept electrons, which can be used to characterize electrophilicity. The HOMO and LUMO density distributions of Fcy and B_nN_n nanocages were shown in Fig. 3. It is worth noting that for Fcy, HOMO is mainly distributed on its O atom and N1 atom, making them more likely interaction sites. For B_nN_n, HOMO is mainly distributed on electronegative N atoms, while LUMO is more distributed on electropositive B atoms. As shown, the E_{HOMO} (E_{LUMO}) of Fcy, $B_{12}N_{12}$, $B_{16}N_{16}$, $B_{20}N_{20}$ and $B_{24}N_{24}$ are calculated to be − 6.35 (−1.43), − 7.93 (−1.05), − 7.61 (−1.25), − 7.72 (−1.31) and − 7.56 (−1.06) eV, hence the E_{bg} are 4.92, 6.88, 6.36, 6.41 and 6.50 eV, respectively. What's more, the E_{bg} results calculated here agree well with those obtained at the B3LYP-D3(BJ)/6–311 G** level (6.87, 6.39, 6.39 and 6.47 eV for $B_{12}N_{12}$, $B_{16}N_{16}$, $B_{20}N_{20}$, and $B_{24}N_{24}$, respectively) [15].

3.2. The most stable adsorption configuration of Fcy onto the B_nN_n

In order to evaluate the potential application of different B_nN_n in detecting or delivering Fcy, the most stable adsorption configuration of Fcy on the surface of B_nN_n were systematically studied, which was obtained at M06–2X-D3/6–311 G* * level. The vibrational stability of these complexes was ensured by their vibrational spectra as shown in Fig. S1, of which all the values obtained are reals without imaginary modes. Structurally, it can be found from Fig. 4**A** that the Fcy is always connected to the B atom of the four-member ring in B_nN_n despite the size of the nanocages. This is consistent with previous reports although a different isoform of $B_{24}N_{24}$ was considered [15]. Meanwhile, though the O atom in Fcy possesses the most negative electrostatic potential of − 52.14 kcal/mol, it is the N1 atom that interacts with B_nN_n. To gain a direct understanding of the interactions between Fcy and B_nN_n, the superposition of ESP mapped vdW surfaces of Fcy and B_nN_n in the B_nN_n-Fcy complexes was shown in Fig. 4**B**. It can be found that in the bonding region, the negative ESP regions around N1 and O atoms in Fcy overlay ideally with the positive ESP regions around B atoms in B_nN_n. Obviously, stacking in this manner can maximize the advantageous overlap of different signs of ESP, ultimately resulting in the most stable structure of the complexes.

The interaction topologies between B_nN_n and Fcy are further

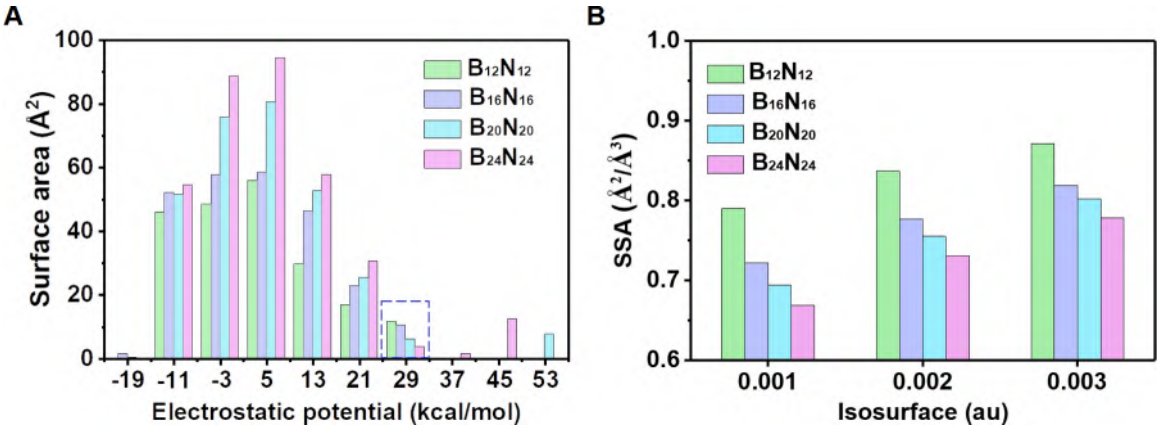

Fig. 2. (A) Area distribution of different ESP intervals and (B) specific surface area (SSA, Å^2/Å^3) for the pristine B_nN_n (n = 12, 16, 20, and 24).

Table 1
The volume (Å^3), surface area (Å^2) and specific surface area (SSA, Å^2/Å^3) of different B_nN_n nanocages based on the vdW surface defined by $\rho = 0.001$, 0.002 and 0.003 au isosurface.

Comp.	Volume (Å^3)			Surface area (Å^2)			SSA (Å^2/Å^3)		
	0.001	0.002	0.003	0.001	0.002	0.003	0.001	0.002	0.003
$B_{12}N_{12}$	264.03	229.17	209.42	208.65	191.85	182.48	0.790	0.837	0.871
$B_{16}N_{16}$	345.04	302.24	277.30	249.12	234.76	227.13	0.722	0.777	0.819
$B_{20}N_{20}$	432.60	380.11	349.29	300.25	287.09	280.07	0.694	0.755	0.802
$B_{24}N_{24}$	513.64	452.97	417.12	343.75	331.17	324.51	0.669	0.731	0.778

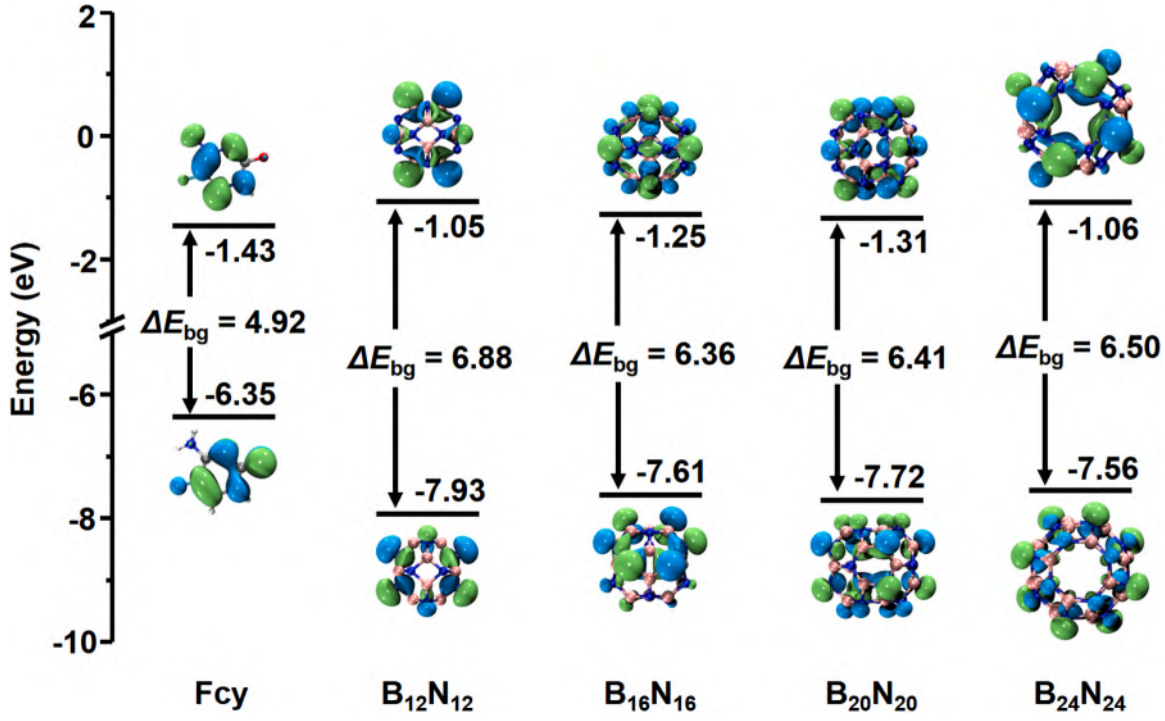

Fig. 3. The HOMO and LUMO density distribution, the calculated HOMO energy (E_{HOMO}, eV), LUMO energy (E_{LUMO}, eV), HOMO-LUMO energy gap (E_{bg}, eV) of the B_nN_n and Fcy at the B3LYP/6–311 G* * level.

identified by the AIM theory, which clarifies the bonding nature based on the topological parameters at the bond critical points (BCPs) [49,50]. The AIM molecular diagram of the B_nN_n-Fcy complexes is shown in Fig. 4**C** and the detailed topology parameters are summarized in Table 2. As presented, there exist B···N bond and N···H bond for all B_nN_n-Fcy complexes, and also N···O bond for the complexes except $B_{12}N_{12}$-Fcy. Among these interactions, the B···N bond has the largest density of all electrons (ρ) and the most negative potential energy density (V_r), indicating it is the main force between B_nN_n and Fcy. Meanwhile, the Laplace of the electron density ($\nabla^2\rho$) of B···N bonds are positive, and its energy density (H_r) are negative, indicating the partially covalent nature of the interaction. And so does the N···H bond in B_nN_n-Fcy complexes (n = 12, 16 and 24). As for the N···O bond, it has positive values of $\nabla^2\rho$ and H_r, thus exhibiting typical electrostatic interaction characteristics. The interactions between Fcy and B_nN_n in gas phase (E_{int}) and aqueous phase ($E_{int\text{-}w}$) were further quantified and plotted in Fig. 5**A**, with relative data summarized in Table S1. Structurally, the negligible RMSD values denote little difference between the optimized structure of B_nN_n-Fcy complexes in gas and aqueous phase. Energetically, the E_{int} of B_nN_n-Fcy (n = 12, 16, 20, and 24) are − 57.91, − 57.28, − 53.99 and − 52.88 kcal/mol, while the $E_{int\text{-}w}$ are − 24.97, − 20.59, − 16.23 and − 15.10 kcal/mol, respectively. It is pronounced that the interaction energy between Fcy and B_nN_n nanocages reduces as the cage size increases, which may attribute to the decreased surface area of the 29 kcal/mol ESP region in B_nN_n that interacts with Fcy (Fig. 2**A**). Additionally, the results suggest that the adsorption behavior of Fcy onto B_nN_n strongly depends on the size of the nanocages, which provides theoretical guidance for the selection of proper carriers for Fcy delivery.

The ESP plots of B_nN_n-Fcy complexes were calculated and displayed in Fig. 6**A.** Significant changes in the electronic distribution of B_nN_n-Fcy complexes are observed as the Fcy part becomes more positive while the B_nN_n part becomes more negative after Fcy adsorption. Thus, the results demonstrate the charge transfers from Fcy to the B_nN_n nanocages. To reveal the electronic structures of the B_nN_n-Fcy complexes and understand the adsorption mechanism of Fcy on the B_nN_n nanocage, the frontier molecular orbitals (HOMO-LUMO) are analyzed and shown in Fig. 6**B-C**. Actually, the adsorption of Fcy substantially affect the distribution of HOMO and LUMO electron clouds of B_nN_n. Specifically, the uniformly distributed HOMO on the N atoms of B_nN_n nanocages have been redistributed to the part near the adsorption sites of Fcy, resulting in the increase in the energy of HOMO. And the LUMO concentrated on the B atoms of B_nN_n are completely transferred to Fcy part in B_nN_n-Fcy, which significantly lowers the energy levels of LUMO in B_nN_n-Fcy. Such a distribution contributes to a significant change in E_{bg} of the system. For example, when Fcy adsorbs onto $B_{12}N_{12}$, the E_{HOMO} of the complex increases from − 7.93 to − 6.73 eV, while the E_{LUMO} decreases from − 1.05 to − 2.58 eV, which leads to the reduction of E_{bg} from 6.88 to 4.15 eV. Similarly, after Fcy adsorption, the E_{HOMO} and E_{LUMO} of $B_{16}N_{16}$-Fcy, $B_{20}N_{20}$-Fcy and $B_{24}N_{24}$-Fcy complexes also changed significantly, with their E_{bg} decreased to 4.03, 4.05 and 4.17 eV, respectively.

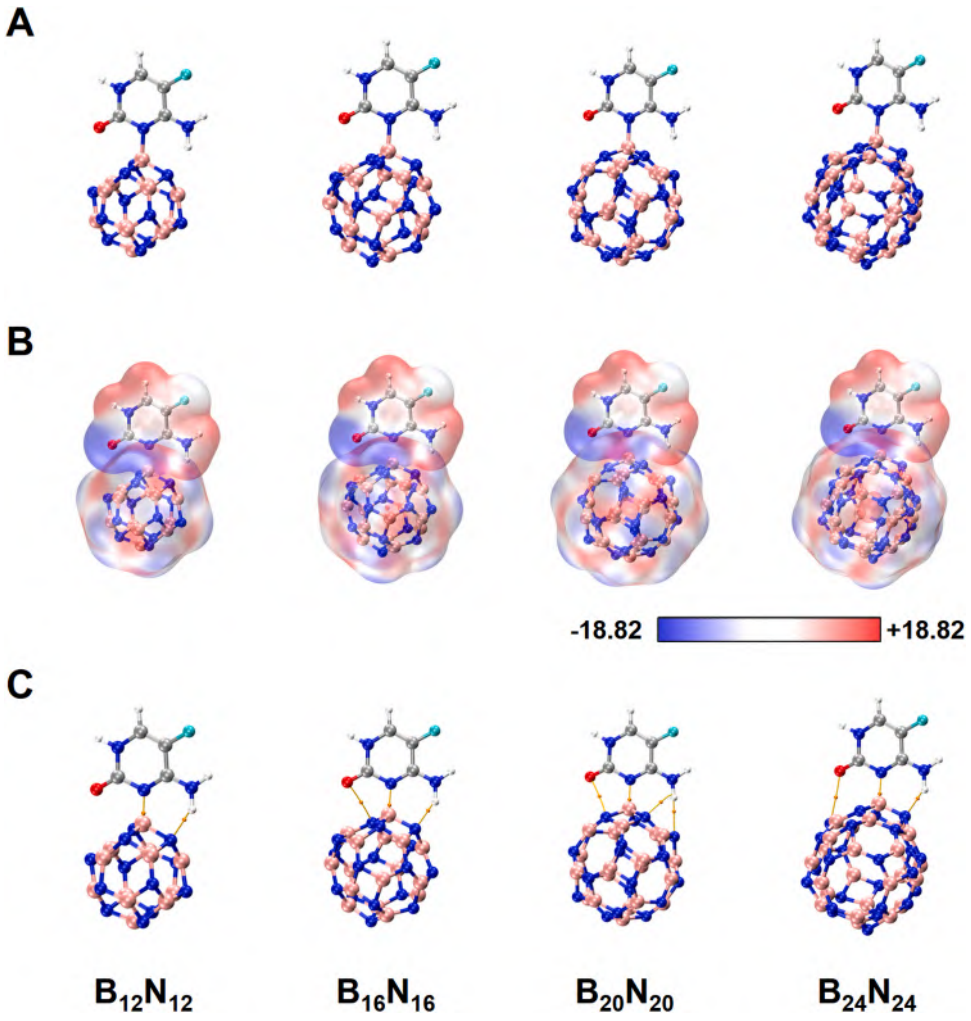

Fig. 4. (A) The optimized configurations of the most stable B_nN_n-Fcy complexes; (B) the superposition of ESP mapped vdW surfaces of Fcy and B_nN_n in the B_nN_n-Fcy complexes (the unit is in kcal/mol); (C) the molecular graph of B_nN_n-Fcy complexes obtained by AIM analyses, the orange line and sphere represent the bond path and the (3, −1) BCP, respectively.

Table 2
Topological parameters, including bond length (d, Å), density of all electrons (ρ), Laplacian of electron density ($\nabla^2\rho$), Lagrangian kinetic energy (G_r), potential energy density (V_r) and energy density (H_r) (all in atomic units) for the optimized B_nN_n-Fcy complexes at the (3, −1) critical points.

Complex	Interaction	d	ρ	$\nabla^2\rho$	G_r	V_r	H_r
$B_{12}N_{12}$-Fcy	B···N	1.63	0.1171	0.3033	0.1574	-0.2390	-0.0816
	N···H	1.80	0.0411	0.1131	0.0322	-0.0361	-0.0039
$B_{16}N_{16}$-Fcy	B···N	1.64	0.1135	0.2856	0.1500	-0.2285	-0.0785
	N···H	1.76	0.0456	0.1143	0.0350	-0.0415	-0.0065
	N···O	2.86	0.0133	0.0545	0.0117	-0.0098	0.0019
$B_{20}N_{20}$-Fcy	B···N	1.63	0.1154	0.3042	0.1559	-0.2357	-0.0798
	N···H	2.32	0.0154	0.0626	0.0130	-0.0104	0.0026
	N···H	2.19	0.0160	0.0597	0.0123	-0.0097	0.0026
	N···O	2.80	0.0141	0.0572	0.0123	-0.0103	0.0020
$B_{24}N_{24}$-Fcy	B···N	1.66	0.1081	0.2667	0.1403	-0.2140	-0.0737
	N···H	1.78	0.0445	0.1149	0.0345	-0.0403	-0.0058
	N···O	2.84	0.0119	0.0485	0.0103	-0.0084	0.0019

Notably, the distribution of frontier molecular orbitals and their energy changes of B_nN_n-Fcy are similar, suggesting that the size of B_nN_n has little influence on the orbitals of these complexes. Besides, the E_{bg} decreased by 39.68%, 36.64%, 36.82% and 35.85% for B_nN_n-Fcy complexes (n = 12, 16, 20, and 24), respectively (Fig. 5**B**). Though decreased in comparison to the pristine B_nN_n nanocages and Fcy (4.92 eV), the E_{bg} values (4.03–4.17 eV) of B_nN_n-Fcy complexes are still greatly larger than the experimentally measured E_{bg} (1.57 eV) of C_{60} [51], suggesting the lower chemical reactivity and high chemical stability of these complexes as drug delivery systems. Moreover, the reduction in E_{bg} stands for the enhancement in conductivity, which may enable the detection of drugs based on electrochemical signals generated during the adsorption process [52]. Therefore, B_nN_n nanocages have high sensitivity to Fcy drug and are expected to be used as Fcy drug sensors.

In addition to E_{HOMO}, E_{LUMO}, E_{bg}, Table 3 also lists the reactivity parameters (μ, η, S and ω) of B_nN_n-Fcy complexes to further characterize the potential of the nanocages as drug carriers. Generally, a smaller η or

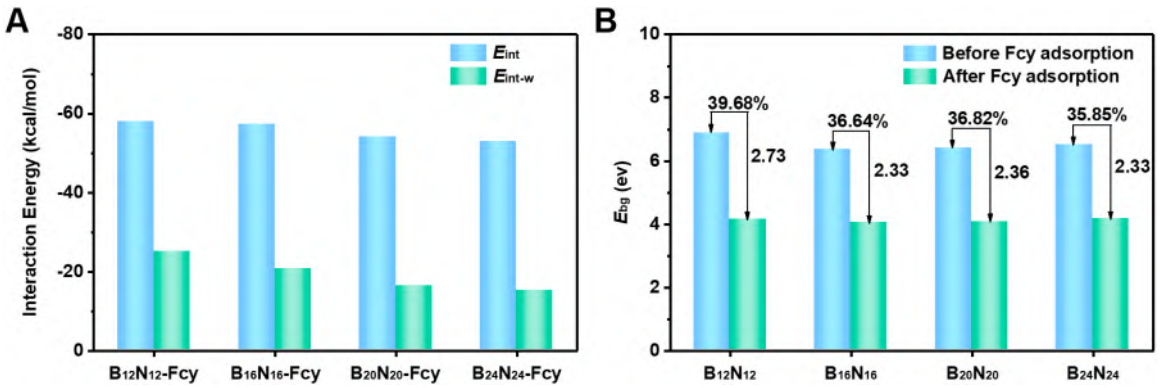

Fig. 5. (A) The interaction energy between Fcy and B_nN_n in gas phase (E_{int}, kcal/mol) and aqueous phase ($E_{int\text{-}w}$, kcal/mol) and (B) HOMO-LUMO energy gap (E_{bg}, eV) changes before and after Fcy adsorption on the B_nN_n.

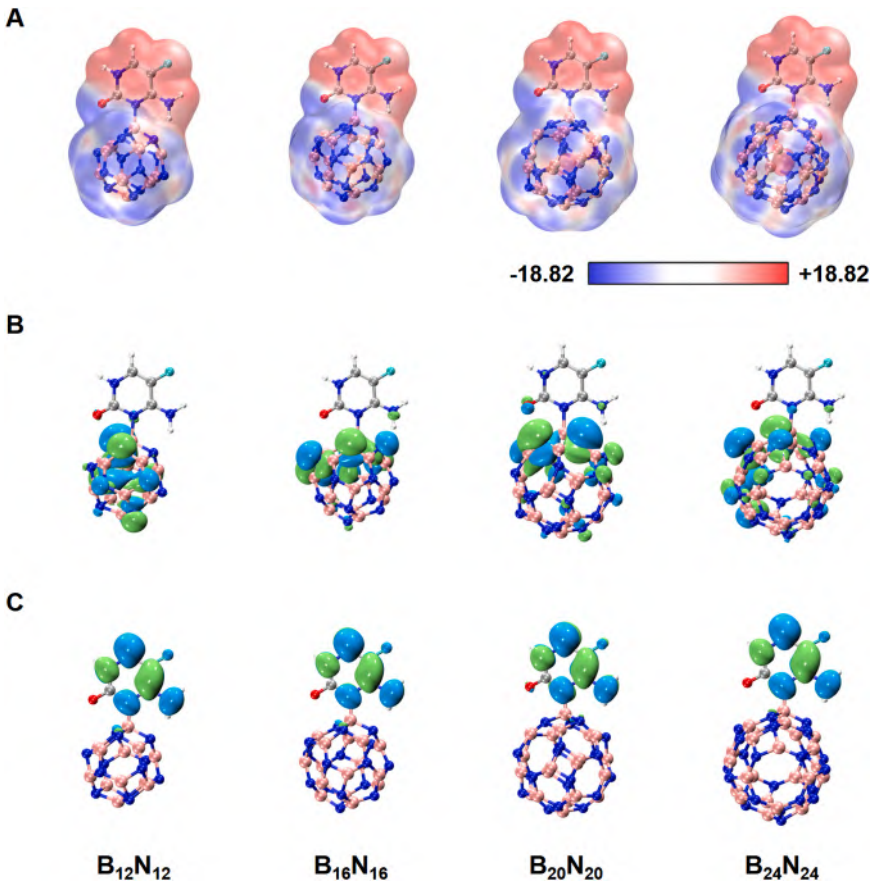

Fig. 6. (A) The ESP-mapped molecular vdW surface, (B) HOMO, and (C) LUMO density distribution of B_nN_n-Fcy (n = 12, 16, 20, and 24).

larger *S* suggests higher reactivity of molecules [53–55]. After Fcy adsorption, η of the B_nN_n-Fcy complexes are reduced and *S* values of these complexes are increased, indicating a more reactive behavior of B_nN_n-Fcy complexes than its original entities. Besides, μ became more negative and ω were enlarged for all B_nN_n-Fcy complexes, which discloses the enhanced ability of B_nN_n-Fcy complexes to gain an additional electronic charge [17]. The dipole moment (DM) can reveal the distribution and intensity of charges, thus making it a useful tool for evaluating the solubility of nanostructures in polar media such as water. The DM of pristine B_nN_n nanocages is equal to zero due to their high symmetry, and the DM value of Fcy is 5.59 Debye. While after Fcy adsorption, the DM of B_nN_n-Fcy complexes is dramatically enhanced to 11.78, 11.96, 12.01 and 12.16 Debye, respectively, implying the increased polarity and better water solubility of these complexes, which is consistent with results from the reactivity parameters. Overall, the above outcomes reveal the formation of B_nN_n-Fcy complexes would improve the distribution of nanoclusters, thereby favorable for the drug delivery in biological media.

3.3. Dynamic adsorption process of Fcy onto the B_nN_n nanocages

As a practical and robust method complementary to experimental methods, MD simulations offer direct insight into the assembly process and a clear understanding of the molecular interactions between different components. Therefore, MD simulations were carried out to study the adsorption process and adsorption capacity of Fcy on the

Table 3
The HOMO energies (E_{HOMO}, eV), LUMO energies (E_{LUMO}, eV), HOMO-LUMO energy gap (E_{bg}, eV), reactivity parameters (μ, η, S and ω, in eV) and dipole moment (DM, Debye) for Fcy, pristine B_nN_n and B_nN_n-Fcy complexes calculated at B3LYP/6–311 G** level.

Compound	E_{HOMO}	E_{LUMO}	E_{bg}	μ	η	S	ω	DM
Fcy	-6.35	-1.43	4.92	-3.89	2.46	0.20	3.08	5.59
$B_{12}N_{12}$	-7.93	-1.05	6.88	-4.49	3.44	0.15	2.93	0.00
$B_{12}N_{12}$-Fcy	-6.73	-2.58	4.15	-4.66	2.08	0.24	5.22	11.78
$B_{16}N_{16}$	-7.61	-1.25	6.36	-4.43	3.18	0.16	3.09	0.00
$B_{16}N_{16}$-Fcy	-6.64	-2.61	4.03	-4.63	2.02	0.25	5.31	11.96
$B_{20}N_{20}$	-7.72	-1.31	6.41	-4.52	3.21	0.16	3.18	0.00
$B_{20}N_{20}$-Fcy	-6.73	-2.67	4.05	-4.70	2.03	0.25	5.44	12.01
$B_{24}N_{24}$	-7.56	-1.06	6.50	-4.31	3.25	0.15	2.86	0.00
$B_{24}N_{24}$-Fcy	-6.78	-2.61	4.17	-4.70	2.09	0.24	5.29	12.16

surface of B_nN_n (n = 12, 16, 20, and 24) nanocages. Snapshots of the B_nN_n systems before and after 20 ns simulations are pictured in Fig. 7. It is can be found that the cage-like structures of B_nN_n were well maintained after a 20 ns simulation, suggesting the adopted force field is applicable for the current system. Meanwhile, the initially randomly distributed Fcy molecules were spontaneously adsorbed on the surface of B_nN_n, which indicates its potential as a drug carrier for Fcy. What's more, different Fcy molecules are adsorbed on the surface of B_nN_n in different configurations (Fig. 7**C**). This reveals that in practical applications, drug molecules are not always adsorbed on the carrier in the most stable configuration due to the interactions between different components, such as drug molecules and solvents.

The radial distribution function (RDF) is widely applied to characterize the intermolecular interactions as it can measure the probability density of a particle appearing at a distance r from the reference atom. Thus, to measure the interactions between B_nN_n and Fcy, the g(r) of B-N1 and B-O pairs were characterized and the results were illustrated in Fig. 8. The $g(r)_{B\text{-}N1}$ and $g(r)_{B\text{-}O}$ exhibit a broad peak from r = 0.27–5.0 nm, suggesting weak intermolecular interactions between Fcy and B_nN_n. Comparably, the $g(r)_{B\text{-}N1}$ is relatively larger than the $g(r)_{B\text{-}O}$, implying the nanocages bind more to the N1 atom than the O atom of the Fcy. Furthermore, the spatial distribution functions (SDF) of N1 and O atoms in Fcy around B_nN_n were plotted in Fig. 9 to give a perspective on the spatial organization of Fcy. The N1 atom in Fcy are distributed around the B atoms of B_nN_n, confirming the specific adsorption of Fcy on B atoms. By comparison, O atoms are always randomly distributed around the nanocage. All these results indicate the B···N bond dominates the interaction between Fcy and B_nN_n though Fcy molecules are adsorbed in different configurations, which is basically consistent with our aforementioned DFT results. It's also worth mentioning that with the cage size increase, the N1 and O atoms are more widely distributed, indicating more adsorption sites on the larger nanocage.

The number of Fcy molecules within the 3.5 Å of B_nN_n (n = 12, 16, 20, and 24) was counted to investigate the size effect on its adsorption capacity. According to Fig. 10**A**, the number of Fcy molecules adsorbed on the B_nN_n surface slowly increased in the first 5 ns of simulation and

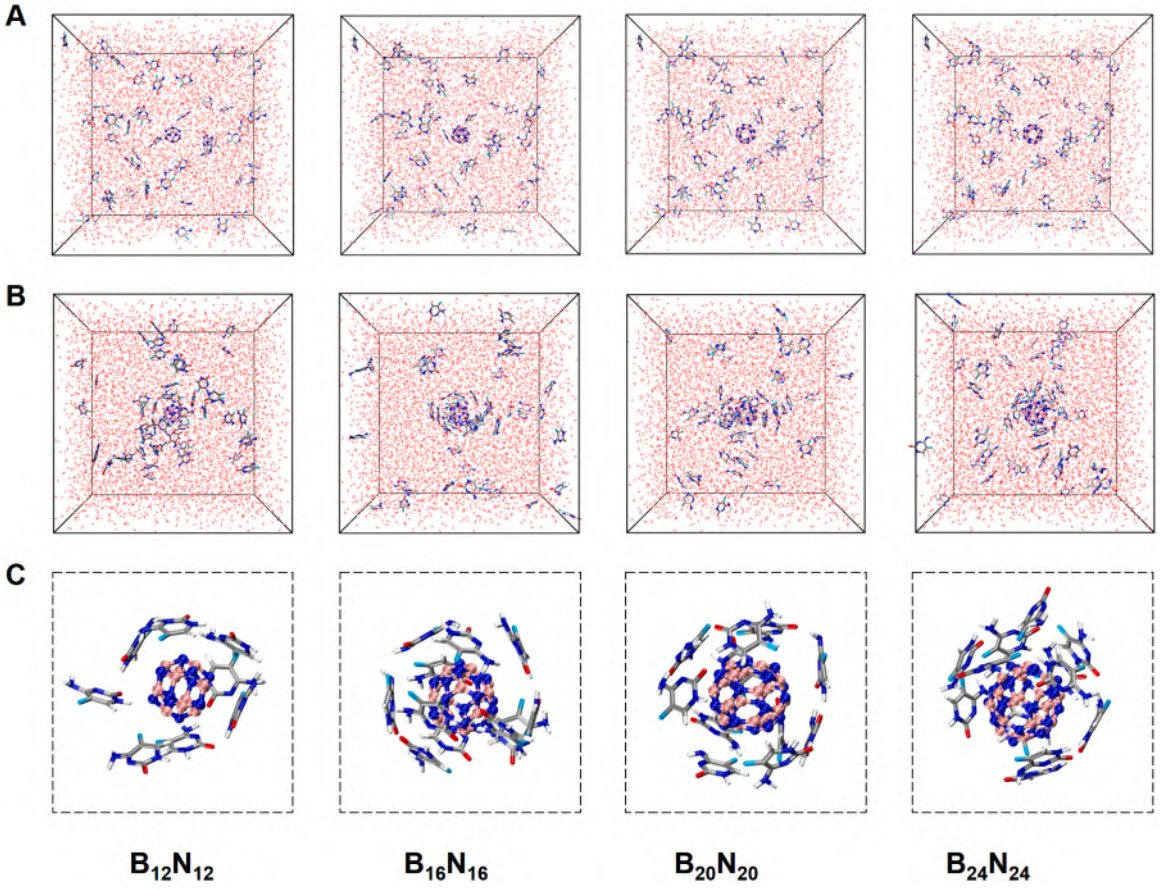

Fig. 7. Snapshots of (A) the initial structure, (B) the relaxed structure and (C) adsorption details for different B_nN_n nanocage adsorb Fcy in MD simulations.

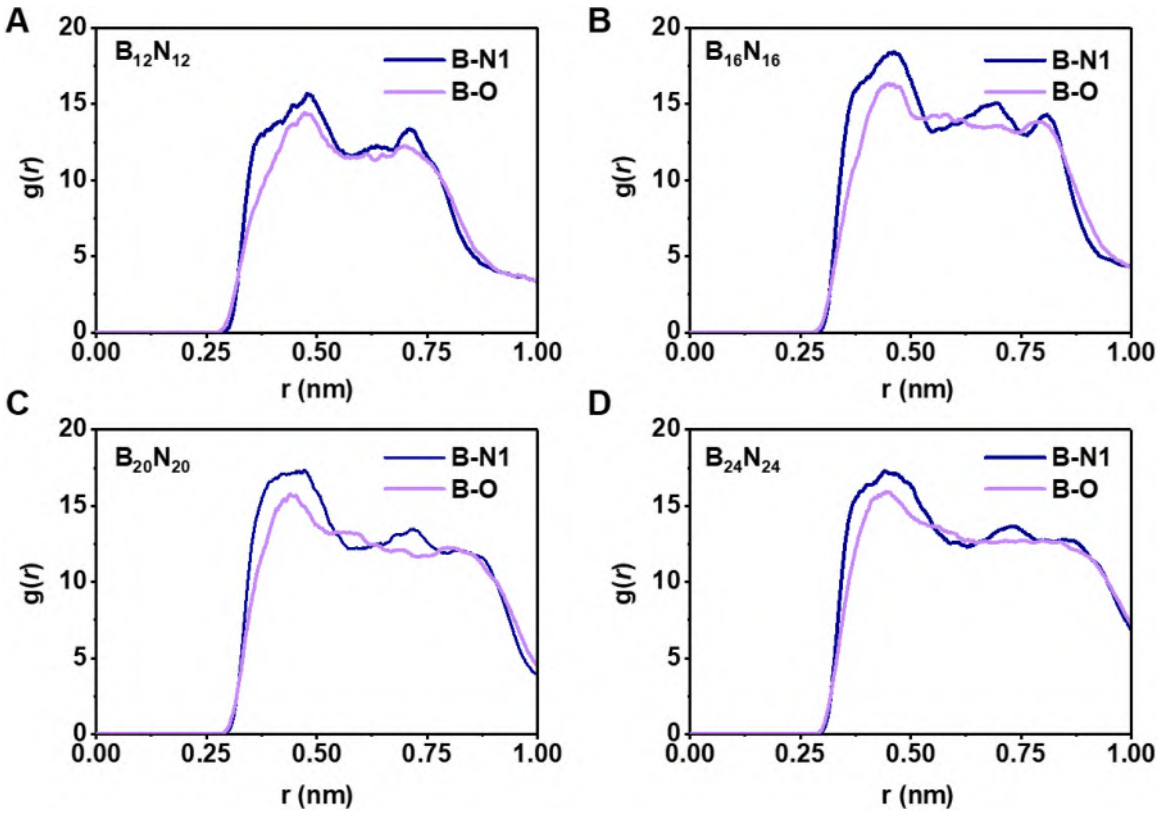

Fig. 8. Radial distribution function (RDF) spectra of B-N1 and B-O atom pairs for different B_nN_n (n = 12, 16, 20, and 24) nanoclusters calculated from the last 10 ns simulation trajectories.

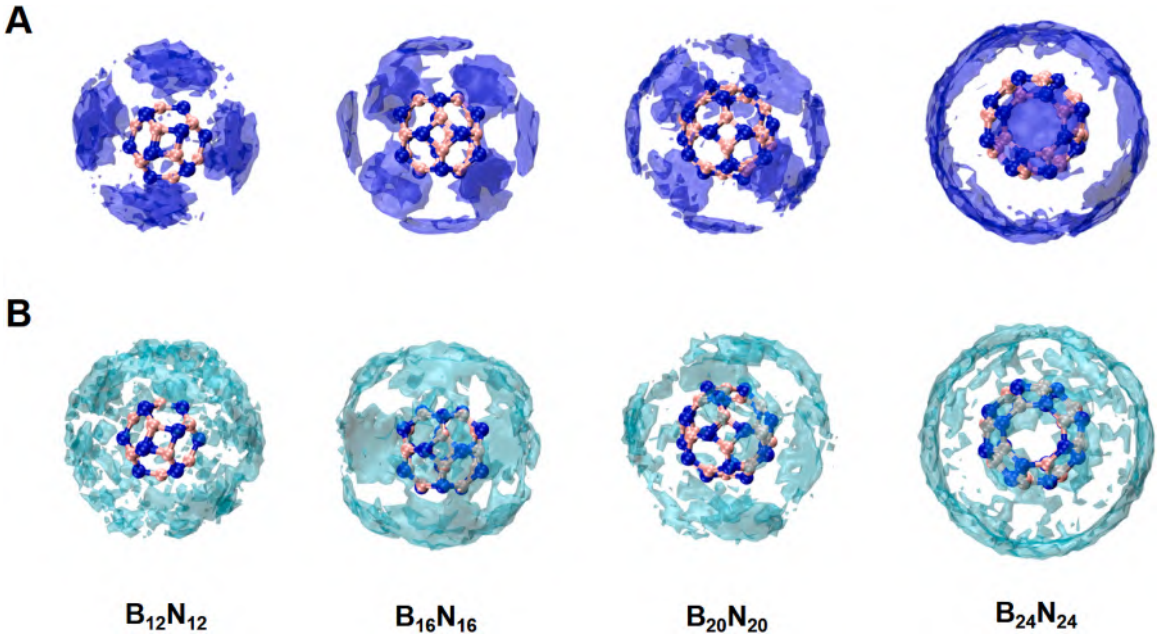

Fig. 9. SDFs of (A) N1 and (B) O atoms from Fcy around different B_nN_n (n = 12, 16, 20, and 24) nanocages obtained from the simulation trajectories.

reached equilibrium after 5 ns. Based on the trajectory of the last 10 ns, the average number of adsorbed molecules for B_nN_n (n = 12, 16, 20, and 24) is calculated to be 7.4, 9.3, 11.1 and 12.7 (Fig. 10**B**), respectively. It is reasonable that larger B_nN_n have more adsorption sites and can adsorb more molecules. After being normalized by the number of $(BN)_{12}$ contained in the molecular formula (*e.g.,* $B_{24}N_{24}$ can be regarded as 2 $(BN)_{12}$), the adsorption capacity of B_nN_n (n = 12, 16, 20, and 24) for Fcy was computed to be 7.4, 7.0, 6.7 and 6.4, respectively, which suggests the adsorption capacity of B_nN_n decreases with the enlargement of the nanocage. To inspect whether the above dependence is also true for other types of drugs, the adsorption capacity of B_nN_n (n = 12, 16, 20, and 24) nanocages for antiviral favipiravir (FPV) and anti-tuberculous isoniazid (INH) drugs was also characterized using the same method. Obviously, the changing rules of the B_nN_n size on the adsorption

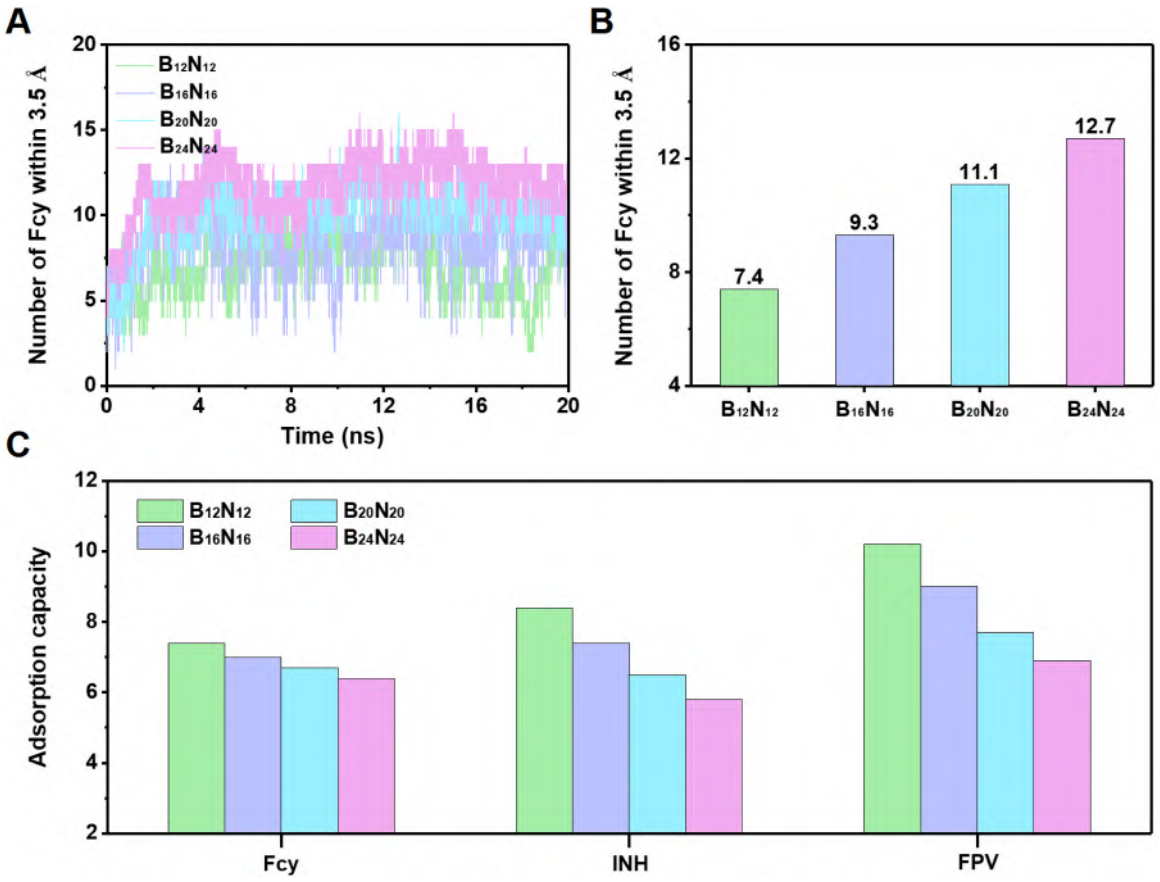

Fig. 10. (A) Evolution of the number of Fcy molecules within 3.5 Å of B_nN_n (n = 12, 16, 20, and 24) with simulation time; (B) averaged number of adsorbed Fcy molecules calculated from the last 10 ns simulation trajectories; (C) the adsorption capacity of B_nN_n (n = 12, 16, 20, and 24) to Fcy, INH and FPV.

capacity of INH and FPV drugs are almost identical to that of Fcy (Fig. 10**C**). Specifically, the adsorption capacity of B_nN_n (n = 12, 16, 20, and 24) for INH (FPV) was counted to be 8.4 (10.2), 7.4 (9.0), 6.5 (7.7) and 5.8 (6.9), respectively. Consequently, the smaller B_nN_n have relatively larger adsorption capacity towards these three drugs, which may attribute to their larger specific surface area. All these results support the idea that the adsorption behavior of Fcy can be tailored by different B_nN_n (n = 12, 16, 20, and 24) nanocages, and suggest that the B_nN_n (n = 12, 16, 20, and 24) nanocage may act as superior carriers to deliver the Fcy drug.

4. Conclusions

In this work, the adsorption behaviors of Fcy on the surfaces of different zero-dimensional B_nN_n (n = 12, 16, 20, and 24) materials were systemically studied based on the DFT and classical MD. After characterizing the structural and electronic properties of different of B_nN_n (n = 12, 16, 20, and 24), it is found that the smaller B_nN_n have a relative larger specific surface area. The most stable adsorption configuration of the Fcy molecule on different B_nN_n nanocages (B_nN_n-Fcy) was obtained to show the perfect complementarity between their EPSs. AIM analysis further indicates that there exist partially covalent interactions and electrostatic interactions between Fcy and B_nN_n (n = 12, 16, 20, and 24), and the partially covalent B···N bonds are the main force between them. For different nanocages, the interaction energy between Fcy and B_nN_n in both gas and aqueous phase decreases as the cage size increases. Meanwhile, large reductions in the HOMO-LUMO energy gap were observed for all B_nN_n-Fcy complexes after Fcy adsorption. Moreover, the results from MD simulations once again demonstrate the B···N bond dominates the interaction between Fcy and B_nN_n although Fcy molecules adopt different adsorption configurations. It also shows that the adsorption capacity of B_nN_n decreases with the enlargement of B_nN_n nanocage. All these results suggest the adsorption behavior of Fcy can be customized by selecting different zero-dimensional B_nN_n (n = 12, 16, 20, and 24) materials, which can thus serve as potential candidates for Fcy drug delivery. Hopefully, the results here would provide meaningful guidance for the development of B_nN_n-based drug delivery systems.

CRediT authorship contribution statement

Xiaocong Yao: Conceptualization, Project administration, Supervision, Funding acquisition. **Ji Mu**: Formal analysis, Visualization, Investigation, Writing – original draft. **Yi Zheng:** Formal analysis, Visualization, Validation, Writing – original draft. **Jiang Wu**: Supervision, Funding acquisition. **Weihua Zhu:** Supervision, Resources. **Kun Wang:** Conceptualization, Data curation, Validation, Funding acquisition, Writing – review & editing.

Declaration of Competing Interest

The authors declare that they have no known competing financial interests or personal relationships that could have appeared to influence the work reported in this paper.

Data availability

Data will be made available on request.

Acknowledgments

This work is supported by the financial support from the National Natural Science Foundation of China (82172226). K.W. is grateful for the financial support from Wenzhou Medical University and X. Y. acknowledges the financial support from general research program of Zhejiang Provincial Department of health (2023KY225).

Appendix A. Supporting information

Supplementary data associated with this article can be found in the online version at doi:10.1016/j.colsurfa.2023.132481.

References

[1] G.D. Brown, D.W. Denning, N.A.R. Gow, S.M. Levitz, M.G. Netea, T.C. White, Hidden killers: human fungal infections, Sci. Transl. Med. 4 (2012), 65rv13.
[2] F. Bongomin, S. Gago, R.O. Oladele, D.W. Denning, Global and multi-national prevalence of fungal diseases-estimate precision, J. Fungi 3 (2017) 1–29.
[3] M.C. Fisher, A. Alastruey-Izquierdo, J. Berman, T. Bicanic, E.M. Bignell, P. Bowyer, M. Bromley, R. Bruggemann, G. Garber, O.A. Cornely, S.J. Gurr, T.S. Harrison, E. Kuijper, J. Rhodes, D.C. Sheppard, A. Warris, P.L. White, J.P. Xu, B. Zwaan, P. E. Verweij, Tackling the emerging threat of antifungal resistance to human health, Nat. Rev. Microbiol. 20 (2022) 557–571.
[4] L.L. Sun, H. Li, T.H. Yan, Y.B. Cao, Y.Y. Jiang, F. Yang, Aneuploidy enables cross-tolerance to unrelated antifungal drugs in Candida parapsilosis, Front. Microbiol. 14 (2023), 1137083.
[5] A. Vermes, Flucytosine: a review of its pharmacology, clinical indications, pharmacokinetics, toxicity and drug interactions, J. Antimicrob. Chemother. 46 (2000) 171–179.
[6] W.W. Hope, P.A. Warn, A. Sharp, S. Howard, M. Kasai, A. Louie, T.J. Walsh, G. L. Drusano, D.W. Denning, Derivation of an in vivo drug exposure breakpoint for flucytosine against Candida albicans and impact of the MIC, growth rate, and resistance genotype on the antifungal effect, Antimicrob. Agents Chemother. 50 (2006) 3680–3688.
[7] F.Z. Bu, Y.M. Yu, Y.L. Shen, L. Liu, C.W. Yan, Z.Y. Wu, Y.T. Li, Cocrystallization-driven self-assembly with vanillic acid offers a new opportunity for surmounting fast and excessive absorption issues of antifungal drug 5-fluorocytosine: a combined theoretical and experimental research, CrystEngComm 24 (2022) 2777–2790.
[8] A. Gómez-López, Antifungal therapeutic drug monitoring: focus on drugs without a clear recommendation, Clin. Microbiol. Infect. 26 (2020) 1481–1487.
[9] C. Dye, Global epidemiology of tuberculosis, Lancet 367 (2006) 938–940.
[10] L. Zhang, F.X. Gu, J.M. Chan, A.Z. Wang, R.S. Langer, O.C. Farokhzad, Nanoparticles in medicine: therapeutic applications and developments, Clin. Pharmacol. Ther. 83 (2007) 761–769.
[11] H. Rahman, M.R. Hossain, T. Ferdous, The recent advancement of low-dimensional nanostructured materials for drug delivery and drug sensing application: A brief review, J. Mol. Liq. 320 (2020), 114427.
[12] S. Angizi, S.A.A. Alem, M. Hasanzadeh Azar, F. Shayeganfar, M.I. Manning, A. Hatamie, A. Pakdel, A. Simchi, A comprehensive review on planar boron nitride nanomaterials: From 2D nanosheets towards 0D quantum dots, Prog. Mater. Sci. 124 (2022), 100884.
[13] M.M. Hasan, A.C. Das, M.R. Hossain, M.K. Hossain, M.A. Hossain, B. Neher, F. Ahmed, The computational quantum mechanical investigation of the functionalized boron nitride nanocage as the smart carriers for favipiravir drug delivery: a DFT and QTAIM analysis, J. Biomol. Struct. Dyn. 40 (2022) 13190–13206.
[14] Z. Zhou, X. Liu, P. Li, $B_{24}N_{24}$ nanocage as an electronic sensor for metronidazole drug: density functional theory studies, J. Mol. Model. 28 (2022), 134.
[15] L. Zhang, X. Cheng, X.H. Li, J.H. Chen, W.M. Sun, A DFT study on the adsorption behavior of antiviral Favipiravir drug on B_nN_n (n = 12, 16, 20, and 24) nanocages: The size effect, J. Mol. Liq. 360 (2022), 119388.
[16] Y.T. Luo, K. Wang, J. Mu, Y.P. Cai, W.H. Zhu, Exploring the adsorption behavior of pyrazinamide on the surface of $X_{12}Y_{12}$(X = B, Al; Y = N, P) nanocages: A in-silico study, J. Mol. Liq. 372 (2023), 121211.
[17] S. Kaviani, S. Shahab, M. Sheikhi, V. Potkin, H. Zhou, A DFT study of Se-decorated $B_{12}N_{12}$ nanocluster as a possible drug delivery system for ciclopirox, Comput. Theor. Chem. 1201 (2021), 113246.
[18] A. Soltani, M.R. Taghartapeh, V. Erfani-Moghadam, M.B. Javan, F. Heidari, M. Aghaei, P.J. Mahon, Serine adsorption through different functionalities on the $B_{12}N_{12}$ and Pt-$B_{12}N_{12}$ nanocages, Mater. Sci. Eng. C. -Mater. Biol. Appl. 92 (2018) 216–227.
[19] Y. Cao, A. Khan, H. Balakheyli, A.N.K. Lup, M. Ramezani Taghartapeh, H. Mirzaei, S. Reza Khandoozi, A. Soltani, M. Aghaei, F. Heidari, S.M. Sarkar, A.B. Albadarin, Penicillamine functionalized $B_{12}N_{12}$ and $B_{12}CaN_{12}$ nanocages act as potential inhibitors of proinflammatory cytokines: a combined DFT analysis, ADMET and molecular docking study, Arab. J. Chem. 14 (2021), 103200.
[20] E. Hosseinzadeh, A. Foroumadi, L. Firoozpour, A DFT study on the transition metal doped BN and AlN nanocages as a drug delivery vehicle for the cladribine drug, J. Mol. Liq. 374 (2023), 121262.
[21] M.C. Flores Bautista, D. Cortés-Arriagada, E. Shakerzadeh, E. Chigo Anota, Acetylsalicylic acid interaction with Boron nitride nanostructures – A density functional analysis, J. Mol. Liq. 355 (2022), 118980.
[22] A. Gholami, E. Shakerzadeh, E. Chigo Anota, M. corazon Flores Bautista, A theoretical perspective on the adsorption performance of pristine and Metal-encapsulated $B_{36}N_{36}$ fullerenes toward the hydroxyurea and nitrosourea anticancer drugs, Inorg. Chem. Commun. 148 (2023), 110326.
[23] A. Gholami, E. Shakerzadeh, E. Chigo Anota, Exploring the potential use of pristine and metal-encapsulated $B_{36}N_{36}$ fullerenes in delivery of β-lapachone anticancer drug: DFT approach, Polyhedron 232 (2023), 116295.
[24] S. Gao, A. Khan, M. Nazari, H. Mirzaei, A.N.K. Lup, M.T. Baei, R. Chandiramouli, A. Soltani, A. Salehi, M. Javan, M.H. Jokar, M. Pishnamazi, A. Nouri, Molecular modeling and simulation of glycine functionalized $B_{12}N_{12}$ and $B_{16}N_{16}$ nanoclusters as potential inhibitors of proinflammatory cytokines, J. Mol. Liq. 343 (2021), 117494.
[25] M.K. Hazrati, Z. Javanshir, Z. Bagheri, $B_{24}N_{24}$ fullerene as a carrier for 5-fluoro-uracil anti-cancer drug delivery: DFT studies, J. Mol. Graph. 77 (2017) 17–24.
[26] M.J. Frisch, G.W. Trucks, H.B. Schlegel, G.E. Scuseria, M.A. Robb, J.R. Cheeseman, G. Scalmani, V. Barone, G.A. Petersson, H. Nakatsuji, X. Li, M. Caricato, A. V. Marenich, J. Bloino, B.G. Janesko, R. Gomperts, B. Mennucci, H.P. Hratchian, J. V. Ortiz, A.F. Izmaylov, J.L. Sonnenberg, Williams, F. Ding, F. Lipparini, F. Egidi, J. Goings, B. Peng, A. Petrone, T. Henderson, D. Ranasinghe, V.G. Zakrzewski, J. Gao, N. Rega, G. Zheng, W. Liang, M. Hada, M. Ehara, K. Toyota, R. Fukuda, J. Hasegawa, M. Ishida, T. Nakajima, Y. Honda, O. Kitao, H. Nakai, T. Vreven, K. Throssell, J.A. Montgomery Jr, J.E. Peralta, F. Ogliaro, M.J. Bearpark, J.J. Heyd, E.N. Brothers, K.N. Kudin, V.N. Staroverov, T.A. Keith, R. Kobayashi, J. Normand, K. Raghavachari, A.P. Rendell, J.C. Burant, S.S. Iyengar, J. Tomasi, M. Cossi, J. M. Millam, M. Klene, C. Adamo, R. Cammi, J.W. Ochterski, R.L. Martin, K. Morokuma, O. Farkas, J.B. Foresman, D.J. Fox, Revision D, Gaussian 09 01 (2009).
[27] D. Li, Y. Kang, J. Li, Z. Wang, Z. Yan, K. Sheng, Chemically tunable DILs: physical properties and highly efficient capture of low-concentration SO_2, Sep. Purif. Technol. 240 (2020), 116572.
[28] J.J. Stewart, MOPAC: a semiempirical molecular orbital program, J. Comput. Aided Mol. Des. 4 (1990) 1–103.
[29] T. Lu, Molclus Program (2016).
[30] S.F. Boys, F. Bernardi, The calculation of small molecular interactions by the differences of separate total energies. Some procedures with reduced errors (Reprinted from Molecular Physics, vol 19, pg 553-566, 1970), Mol. Phys. 100 (2002) 65–73.
[31] G. Scalmani, M.J. Frisch, Continuous surface charge polarizable continuum models of solvation. I. General formalism, J. Chem. Phys. 132 (2010), 114110.
[32] S. Manzetti, T. Lu, Alternant conjugated oligomers with tunable and narrow HOMO-LUMO gaps as sustainable nanowires, RSC Adv. 3 (2013) 25881–25890.
[33] J.M. Crowley, J. Tahir-Kheli, W.A. Goddard, Resolution of the band gap prediction problem for materials design, J. Phys. Chem. Lett. 7 (2016) 1198–1203.
[34] R.F.W. Bader, Atoms in molecules, Acc. Chem. Res. 18 (1985) 9–15.
[35] T. Lu, F.W. Chen, Multiwfn: a multifunctional wavefunction analyzer, J. Comput. Chem. 33 (2012) 580–592.
[36] W. Humphrey, A. Dalke, K. Schulten, VMD: visual molecular dynamics, J. Mol. Graph. 14 (1996) 33–38.
[37] M.J. Abraham, T. Murtola, R. Schulz, S. Páll, J.C. Smith, B. Hess, E. Lindahl, GROMACS: high performance molecular simulations through multi-level parallelism from laptops to supercomputers, SoftwareX 1 (2015) 19–25.
[38] L. Tian, Sobtop, Version 1.0, ⟨http://sobereva.com/soft/Sobtop⟩.
[39] L. Martinez, R. Andrade, E.G. Birgin, J.M. Martinez, PACKMOL: a package for building initial configurations for molecular dynamics simulations, J. Comput. Chem. 30 (2009) 2157–2164.
[40] J. Wang, R.M. Wolf, J.W. Caldwell, P.A. Kollman, D.A. Case, Development and testing of a general amber force field, J. Comput. Chem. 25 (2004) 1157–1174.
[41] C.I. Bayly, P. Cieplak, W. Cornell, P.A. Kollman, A well-behaved electrostatic potential based method using charge restraints for deriving atomic charges: the RESP model, J. Phys. Chem. 97 (2002) 10269–10280.
[42] U. Essmann, L. Perera, M.L. Berkowitz, T. Darden, H. Lee, L.G. Pedersen, A smooth particle mesh Ewald method, J. Chem. Phys. 103 (1995) 8577–8593.
[43] G. Bussi, D. Donadio, M. Parrinello, Canonical sampling through velocity rescaling, J. Chem. Phys. 126 (2007), 014101.
[44] M. Parrinello, A. Rahman, Polymorphic transitions in single crystals: a new molecular dynamics method, J. Appl. Phys. 52 (1981) 7182–7190.
[45] X.Y. Cui, H.S. Wu, Structure and stability of $B_{20}N_{20}$ cluster, Chin. J. Chem. 23 (2005) 117–120.
[46] H.S. Wu, X.H. Xu, J.F. Jia, Structures and stabilities of $B_{24}N_{24}$ cage clusters, Acta Chim. Sin. 62 (2004) 28–33.
[47] T. Oku, A. Nishiwaki, I. Narita, M. Gonda, Formation and structure of $B_{24}N_{24}$ clusters, Chem. Phys. Lett. 380 (2003) 620–623.
[48] J.C. Escobar, M.S. Villanueva, A.B. Hernández, D. Cortés-Arriagada, E.C. Anota, Interactions of $B_{12}N_{12}$ fullerenes on graphene and boron nitride nanosheets: A DFT study, J. Mol. Graph. 86 (2019) 27–34.
[49] I. Ravaei, M. Haghighat, S.M. Azami, A DFT, AIM and NBO study of isoniazid drug delivery by MgO nanocage, Appl. Surf. Sci. 469 (2019) 103–112.
[50] S. Sarfaraz, M. Yar, A.A. Khan, R. Ahmad, K. Ayub, DFT investigation of adsorption of nitro-explosives over C_2N surface: highly selective towards trinitro benzene, J. Mol. Liq. 352 (2022), 118652.
[51] X.B. Wang, C.F. Ding, L.S. Wang, High resolution photoelectron spectroscopy of C60−, J. Chem. Phys. 110 (1999) 8217–8220.

[52] M.M. Kadhim, E.A. Mahmood, V. Abbasi, M.R.P. Heravi, S. Habibzadeh, S. Mohammadi-Aghdam, S.M. Shoaei, Theoretical investigation of the titanium-nitrogen heterofullerenes evolved from the smallest fullerene, J. Mol. Graph. 117 (2022), 108269.
[53] S.R. Pilli, T. Banerjee, K. Mohanty, HOMO-LUMO energy interactions between endocrine disrupting chemicals and ionic liquids using the density functional theory: evaluation and comparison, J. Mol. Liq. 207 (2015) 112–124.
[54] L. Feng, K. Zhong, H.S. Majdi, M. Aallaei, A. Andreevna Rushchitc, Advanced computational study of different boron nitride-based nanospheres for removal of organic contaminants from wastewater system, J. Mol. Liq. 362 (2022), 119740.
[55] S. Kaya, C. Kaya, A new method for calculation of molecular hardness: a theoretical study, Comput. Theor. Chem. 1060 (2015) 66–70.